Mon. Not. R. Astron. Soc. **000**, 1–11 (2010) Printed 28 October 2010 (MN LATEX style file v2.2)

An expanded merger-tree description of cluster evolution

Irina Dvorkin[1⋆] and Yoel Rephaeli[1,2]
[1] *School of Physics and Astronomy, Tel Aviv University, Tel Aviv, 69978, Israel*
[2] *Center for Astrophysics and Space Sciences, University of California, San Diego, La Jolla, CA 92093-0424*

28 October 2010

ABSTRACT
We model the formation and evolution of galaxy clusters in the framework of an extended dark matter halo merger-tree algorithm that includes baryons and incorporates basic physical considerations. Our modified treatment is employed to calculate the probability density functions of the halo concentration parameter, intracluster gas temperature, and the integrated Comptonization parameter for different cluster masses and observation redshifts. Scaling relations between cluster mass and these observables are deduced that are somewhat different than previous results. Modeling uncertainties in the predicted probability density functions are estimated. Our treatment and the insight gained from the results presented in this paper can simplify the comparison of theoretical predictions with results from ongoing and future cluster surveys.

Key words: galaxies: clusters: general - large-scale structure of Universe

1 INTRODUCTION

Formation of galaxy clusters is of central importance for understanding the evolution of the large scale structure (LSS) of the universe. Statistical properties of clusters - deduced from cluster optical, X-ray, and SZ surveys - can be used to determine the basic cosmological parameters - such as the matter density, the normalization (and spectrum) of primordial density fluctuations, and the dark energy equation of state - independently of other methods (CMB power spectrum, galaxy surveys, etc). This can only be achieved if theoretical tools are developed for a quantitative description of the non-linear hierarchical growth of clusters. Hydrodynamical numerical simulations of clusters are currently the most versatile tool for establishing statistical properties of clusters, which are commonly specified in terms of mass functions and scaling relations between their intrinsic properties.

In order to use cluster surveys as cosmological probes it is essential to know how their intrinsic properties - such as formation time, mass and redshift - affect their integrated statistical properties. Clusters are commonly described as virialized spherical systems whose masses are dominated by dark matter (DM) and with isothermal intracluster (IC) gas as their main baryonic mass component. Cluster statistical relations are usually expressed in terms of the mass and the redshift of observation; for example, the resulting scaling of the gas temperature is

$$k_B T \propto M^{2/3} \left[E^2(z)\Delta_V(z)\right]^{1/3}, \qquad (1)$$

where $E(z) = H(z)/H_0$, the Hubble parameter in units of its present value and $\Delta_V(z)$ is the overdensity at virialization.

However, this simple description may not be sufficiently adequate for the description of real clusters. Observations and numerical simulations indicate that DM density profiles are shallower than isothermal at small radii, and steeper than isothermal at large radii, and are characterized by a scaling radius r_s which marks the transition between these two regions (Navarro, Frenk & White 1995, 1996). Although it seems reasonable to assume that the scaling relations are not much affected by the details of the cluster structure, the standard description is not sufficiently accurate since the model parameters - such as r_s - depend on the cluster mass and redshift. Indeed, numerical simulations show that the formation history of clusters affects the DM scaling radius, such that clusters are systematically denser the earlier they formed. Cluster mass concentration is usually quantified in terms of the parameter c, defined as the ratio of the cluster virial radius to the scaling radius, $c = R_v/r_s$. Thus, clusters that form earlier have larger concentration parameters (Wechsler et al. 2002); more generally, other physical properties are also influenced by the cluster formation history.

The assumption of hydrostatic equilibrium is obviously an approximation, since clusters, the largest bound systems, are still forming through mergers of subclumps and accretion. Mergers disrupt the state of thermal equilibrium; during some merger events IC gas temperature and X-ray luminosity are boosted up by factors of up to 3 and 10, respectively, as was demonstrated in a series of numerical simulations by Ricker and Sarazin (2001). More generally, when deriving the standard scaling relations one usually ignores

⋆ E-mail: irina@wise.tau.ac.il

the formation history of the cluster. In the ΛCDM model the LSS formed hierarchically, through consecutive mergers of smaller structures, and thus clusters with roughly the same mass and redshift may have very different merger and formation histories. Indeed, both observations and simulations reveal scatter in the mass-observable relations at a level of $\sim 10\% - 20\%$, which is partly due to the different formation histories (e.g., Wechsler et al. 2002, Vikhlinin et al. 2009a). In order to use these relations to determine the cluster mass function from surveys it is important not only to understand the exact scaling relations, but also to quantify the amount of scatter. Furthermore, uncertainties in the mass-observable relation reduce the precision with which cosmological parameters can be determined (Lima & Hu 2005; Cunha & Evrard 2009).

In current analyses of cluster surveys the scatter in the mass-observable relations has been partly accounted for. Some of this scatter is clearly due to the different dynamical state of the clusters in the survey; unrelaxed systems are sometimes excluded from the analysis. Several studies have indicated that the scatter in the scaling relations is reduced if IC gas temperature is measured by excluding the cluster central region (which is significantly affected by radiative cooling), but the intrinsic scatter in the scaling relations is more difficult to estimate. For example, motivated by insight from simulations, Vikhlinin et al. (2009b) used a constant value of 20% as an estimate for the $T_X - M$ scatter. However, the amount of scatter may depend on the mass and redshift of the cluster.

A meaningful comparison with observational data usually necessitates knowledge of the full probability distribution function (PDF) rather than just the scaling with mass. An example is the case of very large values of the concentration parameter and Einstein radius for several clusters (Broadhurst et al. 2008, Zitrin et al. 2009). Based on results from N-body simulations, the probability of observing clusters with the very high measured values was found to be very low, amounting to a $4-\sigma$ discrepancy with the ΛCDM predictions. The concentration parameter PDF is a crucial component in this analysis (Sadeh & Rephaeli 2008). It is clear that a better understanding of the origin of this PDF is required.

The impact of the formation history on the cluster properties was previously investigated using a series of hydrodynamical simulations (Ricker and Sarazin 2001, Randall and Sarazin 2002, Wik et al. 2008). These authors used simulations of pairs of merging clusters and analysed the impact of recent mergers on IC gas temperature, luminosity, and Comptonization parameter. They found that all these quantities are boosted for a relatively long time following a merger, and calculated the effect of this boost on cosmological parameter estimation. These analyses did not include the full formation history, only the latest merger, and relied on a small number of simulated clusters with different masses. Voit and Donahue (1998) showed that the temperature evolves less rapidly with mass than in the standard analysis when the recent formation approximation is relaxed. They assumed gradual mass accretion throughout the cluster history, and a one-to-one correspondence between the temperature and the virial energy of the cluster.

The statistics of DM halo concentrations and their dependence on the halo formation history were investigated using N-body simulations (Bullock et al. 2001, Wechsler et al. 2002, Neto et al. 2007, Gao et al. 2008, Duffy et al. 2008). This approach provides PDFs of the concentration parameter which account for different formation histories of different halos. Results of these works can then be used to infer the intrinsic scatter in other cluster observables. However, a theoretical approach that is complementary to N-body simulations is needed in order to fully understand the impact of the cluster formation history on its properties. The reliability of the statistical analysis of N-body simulations depends on the simulation volume, which is limited by computational constraints. This can be a severe problem if one is interested in high-mass clusters, which are relatively rare systems. For example, the Millennium Simulation (MS, Springel et al. 2005), the largest cosmological N-body simulation to date, which follows $N = 2160^3$ particles in a periodic box of $L = 500h^{-1}$ Mpc on a side, contains less than 800 relaxed halos with masses above $M_{200} = 1.3 \cdot 10^{14} h^{-1} M_\odot$, and just 8 relaxed halos with masses above $M_{200} = 7.5 \cdot 10^{14} h^{-1} M_\odot$ (Neto et al. 2007, hereafter N07). Moreover, comparison between different simulations is difficult because each utilizes different cosmological parameters and halo finding algorithms. This difficulty is illustrated by the fact that somewhat different mass functions are predicted by different N-body simulations (Jenkins et al. 2001, Sheth & Tormen 2002, Tinker et al. 2008), most likely reflecting the different formation histories predicted by these simulations.

Predicting the full PDFs of the relevant cluster parameters in the context of a theoretical model that can be readily implemented, would allow a more meaningful statistical analysis and the ability to quantify the impact of uncertainties in the values of cosmological and cluster parameters on the main observables deduced from large scale surveys. In this paper we develop a model of cluster formation using analytically computed DM merger trees, with which we trace the formation of clusters through major episodal mergers and continuous accretion. We show that our approach provides an improved physical description in comparison with what can be obtained from standard scaling relations.

This paper is organized as follows. In Section 2 we describe our model of cluster formation. The results of our generalized merger-tree treatment are presented in Section 3 and further discussed in Section 4. Throughout the paper we use the following cosmological parameters: $\Omega_m = 0.25$, $\Omega_\Lambda = 0.75$, $H_0 = 73$ km/s/Mpc, $\sigma_8 = 0.8$.

2 METHODOLOGY

Our description of the growth of galaxy clusters is based on merger trees of DM halos as described numerically by the modified GALFORM code (Cole et al. 2000; Parkinson, Cole & Helly 2008), which was successfully employed to construct semi-analytic models of galaxy formation. The algorithm implements the excursion set formalism, a key aspect of which is the conditional mass function: the fraction of mass $f(M_1|M_2)$ from halos of mass M_2 at redshift z_2 that consisted of smaller halos of mass M_1 at an earlier redshift

z_1

$$f(M_1|M_2)d\ln M_1 = \sqrt{\frac{2}{\pi}}\frac{\sigma_1^2(\delta_1-\delta_2)}{(\sigma_1^2-\sigma_2^2)^{3/2}}\exp\left(-\frac{1}{2}\frac{(\delta_1-\delta_2)^2}{(\sigma_1^2-\sigma_2^2)}\right)\frac{d\ln\sigma_1}{d\ln M_1}d\ln M_1, \quad (2)$$

where $\sigma_i = \sigma^2(M_i)$ is the variance of the linear perturbation field smoothed on scale M_i, and δ_i is the critical density for spherical collapse at redshift z_i. The original GALFORM algorithm is consistent with the Press-Schechter mass function (Press & Schechter, 1974; PS), in the sense that if a grid of trees is rooted at $z = 0$, weighted by their mass abundance according to the PS mass function, then the mass function at higher redshifts again corresponds to PS mass function. The conditional mass function is used to calculate the mean number of progenitors of mass M_1 at redshift $z_1 + dz_1$ of a halo of mass M_2 at $z_2 = z_1$:

$$\frac{dN}{dM_1} = \frac{1}{M_1}\left(\frac{df}{dz_1}\right)_{z_1=z_2}\frac{M_2}{M_1}dz_1 \quad (3)$$

The modified GALFORM algorithm was obtained by making the substitution

$$\frac{dN}{dM_1} \rightarrow \frac{dN}{dM_1}G(\sigma_1/\sigma_2, \delta_2/\sigma_2), \quad (4)$$

where G is referred to as a perturbing function, to be calibrated by comparison with N-body simulations. Parkinson et al. (2008) showed that by fitting the outcome of the algorithm to the results of the MS they obtained halo abundances which are consistent with the Sheth-Tormen mass function (Sheth & Tormen 2002). Thus, the perturbing function G expresses the uncertainty in the choice of the correct mass function. In this work we use the following parametrization of the perturbing function: $G = G_0\,(\sigma_1/\sigma_2)^{\gamma_1}\,(\delta_2/\sigma_2)^{\gamma_2}$, with the parameters $G_0 = 0.57$, $\gamma_1 = 0.38$, $\gamma_2 = -0.01$ taken from Parkinson et al. (2008).

Starting with the specified mass and redshift, the algorithm proceeds back in time, checking after each timestep whether there was a merger; if so, the masses of the merged halos are drawn from the distribution (3). Halos with masses below some resolution limit M_{res} are not resolved, and are accounted for as continuously accreted mass. Further details on the GALFORM algorithm can be found in Parkinson et al. (2008).

In the following sections we describe our model of cluster formation. Since the DM is the dominant mass component of clusters we first study the formation history of cluster-sized DM halos, and then add the IC gas component, study its properties and related scaling relations.

2.1 Modeling the formation of dark matter halos

The calculation begins with the construction of a merger tree for a given final halo mass and redshift. For each tree, we use only the major merger events, that is only those mergers for which $M_>/M_< < q$, whose value is to be determined. The rationale behind this choice is the assumption that the properties of a cluster are largely determined by the violent merger events, during which DM and gas settle in the modified potential well when equilibrium is reestablished. On the other hand, slow accretion of material on the outskirts of the cluster, as well as mergers with low-mass systems (which are treated in an identical manner in this work) do not cause redistribution of the cluster components and do not strongly affect the physical conditions in the cluster center. Thus, we follow the major merger events in the cluster history, and refer to all other processes of mass growth as slow accretion. A typical value of the major merger ratio is $q = 10$; other values will also be considered. The trees were generated up to the redshift $z = z_{fin}$ which depends on the mass resolution of the merger tree algorithm, M_{res}, as discussed below.

The next step is to calculate the density profile of each halo in the tree. To this end, the tree is traced down, beginning with the smaller masses; for each merger event we use energy conservation to calculate the density profile of the merged DM halo. For simplicity we assume NFW (Navarro, Frenk & White 1995) profiles for all the halos at all times:

$$\rho_{DM}(r) = \frac{\rho_s}{x(1+x)^2} \quad (5)$$

where $x = r/r_s = rc/R_v$ is the radial distance expressed in terms of NFW scale radius r_s, c is the concentration parameter, and ρ_s is the mass density normalization constant. Each halo is completely characterized by its mass, redshift and concentration parameter, where halo mass is defined as the mass within the virial radius, $M = \frac{4\pi}{3}R_v^3\rho_c\Delta_V$. All masses are assumed to be in equilibrium, which is presumed to be attained relatively quickly after each merger event, but we do not assume the halos are completely virialized within the virial radius. In fact, the virial ratio $2T/|W|$ approaches 1 at the virial radius only for very large c, while for commonly deduced values of c this ratio is slightly larger than 1 at the virial radius (Cole & Lacey 1996; Łokas & Mamon 2001).

The relation between mass and virial radius depends on redshift, which we identify as the halo formation redshift, z_f, defined as follows. If the halo has undergone a major merger event, we take z_f to be the redshift of the last major merger. This choice is consistent with the main assumption that major mergers largely determine the physics of the halo. For halos that did not experience major mergers at all, and were, according to our interpretation, entirely assembled by minor mergers and continuous accretion, we take z_f to be the redshift at which half of the halo mass had assembled. Difficulty in determining z_f by this prescription is encountered only when the branch of the merger tree terminates when the halo still has *more* than half of its mass (recall that the tree is evolved backwards in time). In GALFORM, the branch is terminated in two cases: either z_{fin} is reached, or the mass of the halo falls below the resolution mass M_{res}. Thus, in order to describe the formation of the smallest halos that constitute the tree, z_{fin} should clearly be chosen well above the expected formation redshift of halos of mass M_{res}. By making this choice we ensure that almost all of the halos in the tree assemble half of their mass before z_{fin} is reached (that is, later in time), and their formation redshift can be traced back by the tree.

To start from the earliest halos in the tree and move forward in time requires specifying their concentration parameters. These are adapted from a fit to a set of N-body

simulations by Bullock et al. (2001)

$$c(M, z_{obs}) = 5\left(\frac{M}{10^{15}h^{-1}M_{\odot}}\right)^{-0.13}\frac{(1+z_f)}{(1+z_{obs})}, \quad (6)$$

where z_f and z_{obs} are the redshifts of formation and observation, respectively. This choice is motivated by the finding of Wechsler et al. (2002) that the concentration parameter scales as $c \sim (1+z_f)/(1+z_{obs})$, although note that their definition of the formation redshift is slightly different than the one adopted here. Although this choice for the initial $c(M, z)$ is somewhat arbitrary, its particular form does not significantly influence the results.

For each merger event, we calculate the total energy of the system before merging, which depends on the concentration parameters of the merging halos, and deduce the concentration parameter of the merged halo from simple energy conservation arguments, motivated by a cluster merger model by Sarazin (2002). The total energy of a system of two halos before merging is:

$$E_{tot,12} = E(M_1) + E(M_2) + U_{12} \quad (7)$$

where $E(M_i)$ are the total energies (potential and kinetic) of each halo and U_{12} is the gravitational energy of the two halos at the point of their largest separation, when they have just become bound and their relative velocity was negligible:

$$U_{12} = -\frac{GM_1M_2}{d_0} \quad (8)$$

The distance d_0, at which the halos became bound, is roughly the mean distance between halos with masses M_1 and M_2 that reside in an overdense region with a scale that corresponds to the final mass $M_f = M_1 + M_2$. We take this distance to be $d_0 = \kappa d$, where $d = R_1 + R_2$, and adopt $\kappa = 5$ as a fiducial value for all halos. This corresponds to a typical distance of several Mpc and a typical relative velocity of several hundreds to a few thousands of km/s, depending on the masses of the merging clusters, which is in accordance with the initial conditions of hydrodynamical cluster merger simulations (Ricker & Sarazin 2001, McCarthy et al. 2007, Lee and Komatsu 2010). Very high values of κ produce unrealistically large initial separations and large relative velocities, while very low values of κ lead to very small initial distances, small relative velocities, and consequently, greatly reduced total energies, which eventually result in very high concentration parameters of the final halo. In other words, κ was chosen so as to yield realistic values of both the initial separation and the final concentration parameter. The dependence of the results on κ is discussed below.

After the two halos merge, the resultant halo accretes matter, so when in turn it merges to form a larger halo, it has more mass than the sum of the masses of its progenitors. We account for the energy of the accreted matter in a very approximate way as follows. Given the masses of the two progenitor halos, M_1 and M_2, and the final mass of the halo, M_p, the total accreted mass is $\Delta M = M_p - (M_1 + M_2) = M_p - M_f$. Numerical simulations of galaxy-sized halos (e. g. Wang et al. 2010) seem to indicate that the accreted material is distributed in the halo outer region. This is quite likely the case also in cluster-sized halos, so we can estimate the energy due to the accreted mass by writing

$$U_{acc} = -\frac{G(M_1 + M_2)\Delta M}{R_f}, \quad (9)$$

where R_f is the virial radius of the halo with mass $M_f = M_1 + M_2$ that formed just after the merger. In evaluating U_{acc} we assume that the accreted mass constitutes a relatively small fraction of the final halo, and that equation (9) provides a simplified description of the accretion process.

We then have for the total energy of the system prior to merging

$$E_{total} = E_{tot,12} + U_{acc} \quad (10)$$

This energy is attributed to the resulting merged halo; we assume no mass is lost in the process. By equating E_{total} with the gravitational and potential energy of the resulting halo, which depend on its concentration parameter, we can deduce the latter. This process is repeated for each halo in the tree, until arriving at the bottom - the most massive halo. At the end of this process we obtain the concentration parameter for the given mass and for one tree, i.e. one realization of the halo history. Generating a large number of trees gives an estimate of the PDF of $c(M)$.

2.2 Modeling the intracluster gas

In our modeling of IC gas we assume that it constitutes a small fraction of the total cluster mass, and that it does not significantly affect the evolution of the cluster. We assume that the gas has a polytropic equation of state with an adiabatic index Γ, such that the gas density and pressure are related through:

$$P = P_0(\rho/\rho_0)^{\Gamma} \quad (11)$$

The solution of the equation of hydrostatic equilibrium for a polytropic gas inside a potential well of a DM halo with an NFW profile is (Ostriker, Bode, & Babul 2005):

$$\rho(x) = \rho_0\left[1 - \frac{B}{1+n}\left(1 - \frac{\ln(1+x)}{x}\right)\right]^n, \quad (12)$$

where $n = (\Gamma - 1)^{-1}$ and B is given by:

$$B = \frac{4\pi G\rho_s r_s^2 \mu m_p}{k_B T_0}, \quad (13)$$

and μm_p is the mean molecular weight. Thus, B depends on the concentration parameter through ρ_s and r_s (see equation (5)). The temperature profile is then

$$T(x) = T_0\left[1 - \frac{B}{1+n}\left(1 - \frac{\ln(1+x)}{x}\right)\right] \quad (14)$$

As a boundary condition we assume that the gas pressure at the virial radius obeys $P_{gas} = f_g P_{DM}$ where f_g is the gas mass fraction and $P_{DM} = \rho_{DM}\sigma^2$ (Ostriker et al. 2005). We obtain σ^2, the DM (3D) velocity dispersion, by solving the Jeans equation for the NFW potential. We expect this particular choice for the boundary condition to have a minor influence on the results, as discussed in Section 4.

For each merger tree we obtain the concentration parameter and the virial radius of the final halo, as described above. Taking the observationally deduced value for the adiabatic index, $\Gamma = 1.2$, and imposing the above boundary

condition to obtain the constant B fully determines the temperature profile. By assuming a specific gas mass fraction we also obtain the full density profile. Repeating this procedure for a large number of trees provides an estimate of the PDFs of the various physical parameters as a function of the cluster mass and the redshift of observation.

In order to derive scaling relations we define the mean cluster temperature as the emission-weighted value

$$T_{ew} \equiv \frac{\int \Lambda(T)\rho_g^2 T dV}{\int \Lambda(T)\rho_g^2 dV}, \quad (15)$$

where integration is over the cluster volume, and the temperature dependence of the cooling function is approximately $\Lambda(T) \propto \sqrt{T}$. Similarly, X-ray luminosity is approximated by:

$$L_X = \int \left(\frac{\rho_g}{\mu m_p}\right)^2 \Lambda(T) dV. \quad (16)$$

Knowledge of the gas temperature allows also calculation of the Comptonization parameter, y, defined as

$$y = \int \left(\frac{k_B T_e}{m_e c^2}\right) n_e \sigma_T dl, \quad (17)$$

where the integral is taken along the line of sight to the cluster, σ_T is the Thomson scattering cross section (and the electron temperature T_e is assumed to equal the gas temperature). The measured SZ intensity (change) is approximately proportional to the integrated Y-parameter, given by the integral of y over the angle the cluster subtends on the sky

$$Y = \int y d\Omega \quad (18)$$

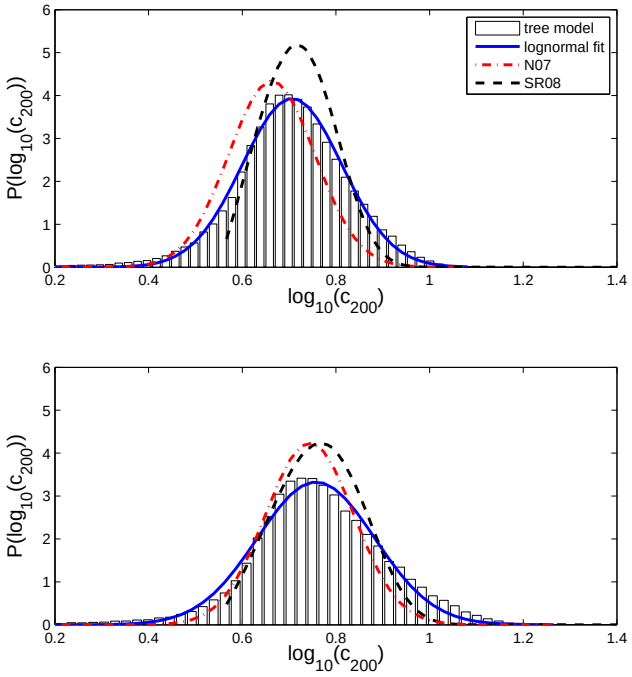

Figure 1. Concentration parameter probability distribution function (PDF) as predicted by the merger-tree model (bars), the lognormal fit to this PDF (solid line), a distribution extracted from the MS by N07 (dot-dashed line) and the prediction of SR08 (dashed line). *Upper panel:* $M = 4 \times 10^{14} h^{-1} M_\odot$ for the merger tree model and a corresponding range of $M_{200} = 10^{14.25} - 10^{14.75} h^{-1} M_\odot$ from the MS. *Lower panel:* $M = 6 \times 10^{13} h^{-1} M_\odot$ for the merger tree model and a corresponding range of $M_{200} = 10^{13.63} - 10^{13.88} h^{-1} M_\odot$ from the MS.

3 RESULTS

3.1 Model parameters

The model contains several physical parameters, and two numerical (code-specific) parameters - the number of tree realizations used to estimate the PDFs and the resolution mass of the merger tree. We shall discuss the latter parameters here and defer the discussion of the physical parameters to subsequent sections.

A key objective of our model is to determine the PDF of the concentration parameter and IC gas temperature by generating a large number of merger tree realizations N. We have found that taking $N = 5 \cdot 10^4$ is sufficient to obtain convergent results - taking larger N does not change the PDF by more than a fraction of a percent. In what follows, we show histograms of 50 binned values obtained from $5 \cdot 10^4$ merger trees.

As noted earlier, a resolution mass needs to be selected for each tree. This mass is the smallest building block used in the tree. By sampling different values of the resolution mass, we find that M_{res} has to be at least 3 orders of magnitude below M, the final mass for which the tree is built, while taking smaller values of M_{res} does not affect the results: for the mass range we consider, the mean value of c changes by no more than 1% when the resolution mass is lowered from $M_{res} = 10^{-3} M$ to $M_{res} = 10^{-4} M$. The value of M_{res} determines z_{fin}, as discussed above.

3.2 PDF of halo concentration

The basic outcome of the model is the concentration parameter of the DM halo at a given redshift of observation. Each merger tree results in a slightly different concentration parameter, which depends on the particular structure of the merger tree. Thus, in the limit of a large number of tree realizations the distribution of formation histories provides a PDF of the concentration parameter. The PDF of c for $M = 4 \times 10^{14} h^{-1} M_\odot$ at $z = 0$ is shown in Figure 1 (upper panel). A log-normal distribution provides a reasonable fit, with $< \log_{10} c >= 0.706$ and $\sigma_{\log_{10} c} = 0.106$. The width of the distribution is comparable with the value obtained by N07 for a population of relaxed halos in the corresponding mass range $M_{200} = 10^{14.25} - 10^{14.75} h^{-1} M_\odot$ seen in the MS: $< \log_{10} c >= 0.663$ and $\sigma_{\log_{10} c} = 0.092$. The distribution for a lower mass of $M = 6 \times 10^{13} h^{-1} M_\odot$ is shown in the lower panel, along with a corresponding distribution for halos in the MS in the mass range of $M_{200} = 10^{13.63} - 10^{13.88} h^{-1} M_\odot$. For this mass we obtain $< \log_{10} c >= 0.758$ and $\sigma_{\log_{10} c} = 0.106$ from the log-normal fit, compared with $< \log_{10} c >= 0.744$ and $\sigma_{\log_{10} c} = 0.094$ for the halos in the MS. We note that the mass correspondence is only approximate, since the relation between M_{200} and M_v for a given halo depends on its concentration parameter.

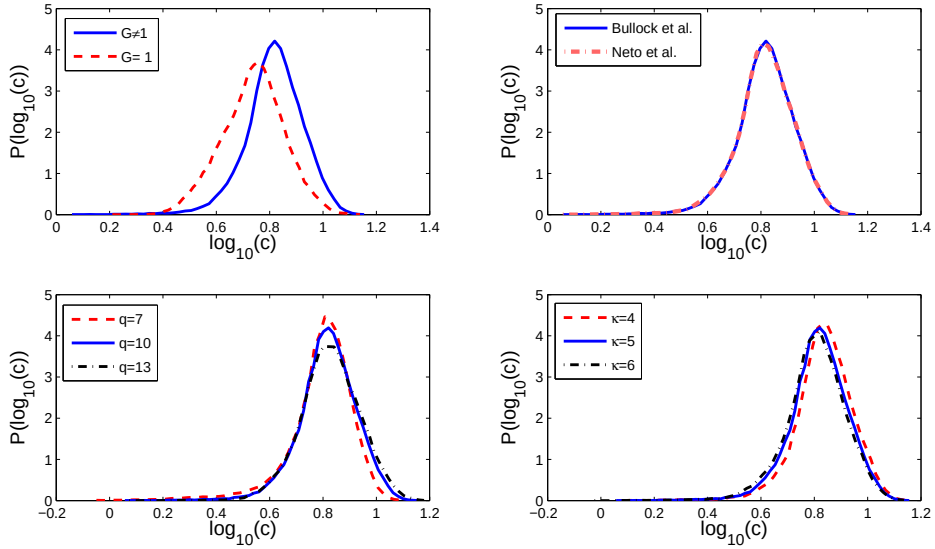

Figure 2. PDF of the concentration parameter from the merger-tree model for $M = 10^{15}h^{-1}M_{\odot}$ at $z = 0$ with different model parameters, as discussed in the text. Shown in the *Left upper panel* is the dependence on the mass function through the perturbing function G (see equation (4)), the dependence on the initial conditions for $c(M, z)$ for the earliest halos in the tree in the *Right upper panel*, the dependence on the major merger parameter $q = M_{>}/M_{<}$ in the *Left lower panel*, and the dependence on $\kappa = d_0/d$ (which parametrizes the initial distance between halos that are about to merge) in the *Right lower panel*.

For comparison, a semi-analytical calculation adapted from Sadeh and Rephaeli (2008; SR08) is also shown. This latter treatment was based on an analytical distribution of formation times and a relation between the formation time and concentration parameter deduced from numerical simulations by Wechsler et al. (2002). The merger tree model predicts slightly lower concentration parameters and a slightly broader distribution function. It is important to note that both treatments result in quite similar PDFs that are also consistent with the results of numerical simulations, despite of the competely different assumptions made in each of these approaches.

As mentioned earlier, the uncertainty in the correct form of the mass function is quantified by the perturbing function G (see equation (4)). Figure 2 (left upper panel) shows how the concentration parameter changes when the merger tree is computed with and without the perturbing function G. As expected, the concentration parameter tends to be larger in the former case, reflecting the earlier formation time of halos in the MS as compared with the extended Press-Schechter formalism (Wechsler et al. 2002). This result illustrates the rather strong dependence of the PDF of c on the mass function. This dependence has to be accounted for when comparing results from observations and numerical simulations.

The initial conditions of the tree are the concentration parameters of the earliest halos. As indicated earlier, the particular choice of $c(M, z)$ for the earliest halos does not appreciably affect the final value of c, as long as this choice is reasonable. For example, Figure 2 (right upper panel) shows the probability distributions of c with the initial $c(M, z)$ taken from the fit in equation (6), and a different fit adapted from the results of N07:

$$c = 5.26 \left(\frac{M}{10^{14}h^{-1}M_{\odot}}\right)^{-0.1} \frac{1+z_f}{1+z_{obs}} \qquad (19)$$

It can be seen that there is no significant change in the distribution function. The influence of these initial condition on the results is further discussed at the end of section 3.3.

The structure of the tree, and hence the calculation of c, depends somewhat on the chosen ratio for major mergers, $q = M_{>}/M_{<}$. This dependence is shown in Figure 2 (left lower panel); the choice of q is guided by several physical considerations. On the one hand, it should not be too small, because this would take into account only nearly equal-mass mergers. Hydrodynamical simulations (Wik et al. 2008, McCarthy et al. 2007) show that mergers with mass ratios as high as $q = 10$ still lead to strong disruption of equilibrium in the inner cluster region, and would thus need to be treated as major merger events in our approach. The dynamical impact of taking higher values of q has not been explicitly explored in hydrodynamical simulations. Accordingly, we selected this value to be the highest value of q above which the mergers are approximated as continuous mass accretion.

The value of κ, which determines the separation at which two halos become bound, also influences the results quite appreciably. Figure 2 (right lower panel) shows that deviations from the fiducial value of $\kappa = 5$ can shift the distribution of c due to changes in cluster initial energies. As discussed earlier, the value $\kappa = 5$ was chosen so as to produce realistic distances between clusters that are about to merge, and is consistent with estimates of relative velocities of merging clusters (Lee and Komatsu 2010).

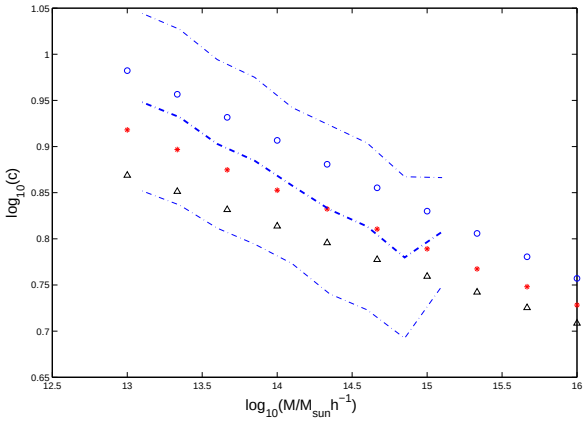

Figure 3. $c-M$ relation at $z=0$ (circles), 0.5 (stars) & 1 (triangles). The thick line shows the results of N07 with the dispersion in the logarithm of c indicated by the thin lines. The mass dependence is consistent with the results of the MS.

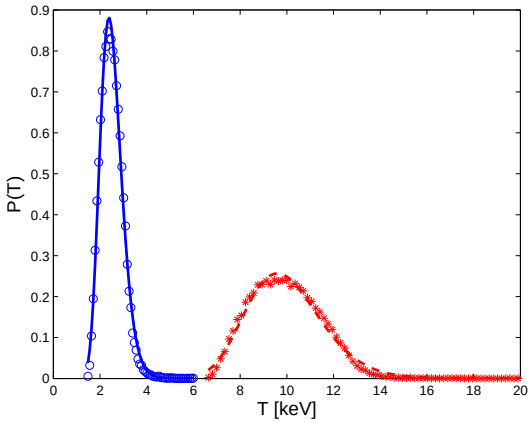

Figure 4. IC gas temperature PDFs predicted by the merger-tree model and best fits to a log-normal distribution for $10^{14}h^{-1}M_{\odot}$ (circles, solid line), and for $10^{15}h^{-1}M_{\odot}$ (asterisks, dashed line). These distributions exhibit a characteristic sharp cutoff at low temperatures and a long high-temperature tail, as expected.

3.3 Scaling relations of the concentration parameter

The expectation values of the distribution functions from the previous sections provide the concentration parameter averaged over formation histories. It is obviously important to follow the redshift evolution of c and its distribution with the final mass. Figure 3 shows the $c-M$ relation for several redshifts of observation. The results can be well described by the scaling relation $c \propto M^{-\alpha}$, with strong redshift dependence of α, ranging from $\alpha = 0.075$ for $z=0$ to $\alpha = 0.054$ for $z=1$, so that the dependence of c on mass is weaker for higher redshifts. This likely represents the fact that c depends on mass through the formation redshift, and the difference in formation redshifts for different masses observed at $z=0$ is larger than for different masses observed at a higher redshift. This flattening of the mass-concentration relation at high redshifts is also seen in numerical simulations (Duffy et al. 2008, Gao et al. 2008), although our predictions for α are slightly lower at low redshift and slightly higher at high redshift than those of Duffy et al. Figure 3 also shows the results of N07 for halos at $z=0$ extracted from the MS (thick line) along with the $1-\sigma$ distribution widths (thin lines). These results of the MS are consistent with the predictions of the merger-tree model, although there seems to be a systematic offset between the respective results from these two very different studies.

The dependence on the cluster observation redshift, which is often taken to be $c \sim (1+z_{obs})^{-\gamma}$ with $\gamma = 1$, is also found to be much weaker and mass-dependent, ranging from $\gamma = 0.38$ for $M = 10^{13}h^{-1}M_{\odot}$ to $\gamma = 0.24$ for $M = 10^{15}h^{-1}M_{\odot}$. This results in slower redshift evolution than found by Duffy et al, but is more consistent with the findings of Gao et al. for massive halos extracted from the MS, especially for masses around $M \sim 10^{14}M_{\odot}$ for which our result $\gamma = 0.31$ coincides with the evolution seen by Gao et al. (note, however, that these authors use the Einasto profile to describe DM halos).

In general, the scaling relations deduced from numerical simulations are effectively weighted by the mass function, and, since the latter has a sharp cutoff at about the typical mass of a galaxy cluster, mainly reflect the structure of smaller, galaxy-sized halos at low redshifts. Extrapolations of the results of such simulations cannot faithfully describe the structure of massive halos at high redshifts, as pointed out by Gao et al. Although we use the results of Bullock et al. as the initial conditions for the merger tree - equation (6) - this choice is justified because our final results are not sensitive to the exact form of these initial conditions. In addition, the initial halos in the merger tree have smaller masses, in the range explored by Bullock et al.

Full investigation of the $c-M$ relations and their redshift evolution neccesitates the use of numerical simulations targeted at massive, cluster-sized halos. We plan to continue our study in this direction using the hydrodynamical AMR code *Enzo*.

3.4 PDF of IC gas temperature

Since the temperature of IC gas is used as a mass proxy in cluster surveys, its PDF is of great observational importance. We have computed this distribution as outlined above. Figure 4 shows the PDFs of the emission-weighted temperature for cluster masses $M = 10^{15}h^{-1}M_{\odot}$ and $M = 10^{14}h^{-1}M_{\odot}$ at $z=0$.

As expected, the PDF exhibits a long high-temperature tail which corresponds to those clusters that were formed atypically early. At low temperatures, on the other hand, there is a sharp cutoff that corresponds to clusters that formed close to their observation redshift. A log-normal distribution provides a good approximation to the temperature PDF below $M \sim 2\cdot 10^{15}h^{-1}M_{\odot}$, as can be seen in Figure 4. The width of the distribution is $\sigma_{\log_{10}c} = 0.07$ for $10^{15}h^{-1}M_{\odot}$ and $\sigma_{\log_{10}c} = 0.08$ for $10^{14}h^{-1}M_{\odot}$.

3.5 Temperature scaling relations

Scaling relations of the gas temperature with cluster redshift, mass, and X-ray luminosity are commonly used in statistical analyses of the cluster population and in the use of

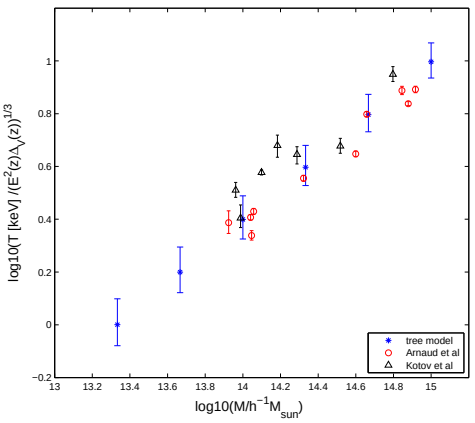

Figure 5. Mass-temperature scaling relation at $z = 0$ for the merger-tree model (stars) and from observations (circles and triangles).

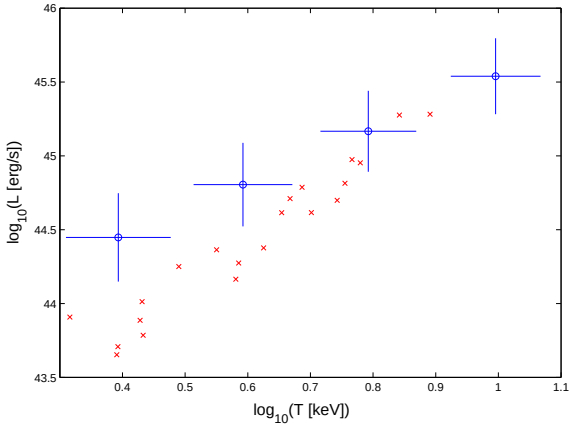

Figure 6. X-ray luminosity vs. emission-weighted temperature (circles with error bars), where the error bars correspond to the disrtibution width in the logarithm of the luminosity and temperature, respectively. A constant gas mass fraction $f_g = 0.1$ was assumed. Also shown are measurements of the bolometric luminosity vs. spectroscopic temperature from Pratt et al. (crosses).

clusters as cosmological probes. Most useful is the $T - M$ relation which can be determined from the probability distribution functions. In Figure 5 we show the emission-weighted temperature versus mass for clusters at $z = 0$. The temperature was calculated using equation (15). Blue stars represent expectation values of the PDFs, with errorbars indicating the distribution variance. The red circles are measurements of a sample of clusters from Arnaud, Pointecouteau & Pratt (2005), and the black triangles are measurements of another sample by Kotov & Vikhlinin (2005), where redshift correcting factors have been included for both samples. The merger tree results are best-fit with the relation $T \propto M^{0.6}$, which is very close to the theoretical relation obtained for an isothermal sphere, $T \propto M^{2/3}$. It can be seen that the results and the expected scatter are consistent with observations. Note though the different definitions of mass (M_{200} in Arnaud et al., M_{500} in Kotov & Vikhlinin) and temperature (spectral temperature in both Arnaud et al. and Kotov & Vikhlinin).

The observational results suggest that the variance of the temperature PDF can be seen to represent the amount of scatter that is expected in observed clusters due to their different formation history. Note that the error in the measured temperatures is small compared to the scatter, which is slightly larger than the predicted intrinsic scatter, as expected, since it has additional contributions. For example, not all clusters are fully relaxed and spherical, etc. We find that the temperature scales as a power-law in mass at all redshifts, $T \propto M^{\zeta}$; however ζ varies somewhat with redshift, from 0.6 for $z = 0$ to 0.63 for $z = 2$, which results in slower evolution compared to the simple scaling $\zeta = 2/3$. We note that the *minimal* possible temperature of a given mass - the low-temperature endpoint of our PDF - scales as $T_{min} \propto M^{0.65-0.66}$ in our model for all redshifts, in much better agreement with the standard value. Indeed, the standard treatment assumes that the halo is observed immediately after it had formed, which is precisely the situation described by the low-temperature end of the PDF. The expectation value, however, is affected by the width of the PDF, which also depends on mass.

The predicted redshift dependence of T is another key relation whose knowledge is important as it reflects on cluster evolution, and its approximate analytic form is needed in comparisons with results of cluster X-ray and SZ surveys. The basic redshift scaling of the temperature is contained in the relation $T \propto [E^2(z)\Delta_V(z)]^{\lambda}$, where λ varies somewhat with mass, from $\lambda = 0.2$ for $M = 10^{13}h^{-1}M_{\odot}$ to $\lambda = 0.26$ for $M = 10^{15}h^{-1}M_{\odot}$. Thus, $T(z)$ is less steep than in the standard relation (1), where $\lambda = 1/3$. In addition, the slope of this scaling relation differs with mass, hinting that the temperature might not be a separable function in terms of mass and redshift. The dependence of these results on the model parameters is discussed in Section 3.8.

The luminosity-temperature relation is an important probe of the IC gas. In the framework of the presented approach it can be used to test the validity of the simple polytropic model. Figure 6 shows the luminosity-temperature relation obtained from the merger-tree model, as well as X-ray measurements of a sample of clusters by Pratt et al. (2009). There is reasonable agreement with the data in the high-temperature end, with the distribution width approximately corresponding to the scatter in the measured values, but the model clearly overpredicts the luminosity of low-temperature clusters. One reason for this could be non-constant gas mass fraction which, as hinted by observations, is lower in low-mass systems. The dependence of the gas mass fraction on mass and redshift could also be related to additional physical processes in the IC gas, such as radiative cooling and feedback from supernovae and AGN.

3.6 Integrated Comptonization parameter

Having determined the IC gas temperature and density profiles (as outlined above), we can now compute another key observable - the integrated Comptonization parameter. To do so, we also need to specify the gas mass fraction, which is taken to be $f_g = 0.1$ for all halos. Figure 7 shows the PDF of Y; it exhibits the same general features as the temperature distribution, a sharp cutoff at low Y, and a long exponential tail at high values, largely due to clusters that

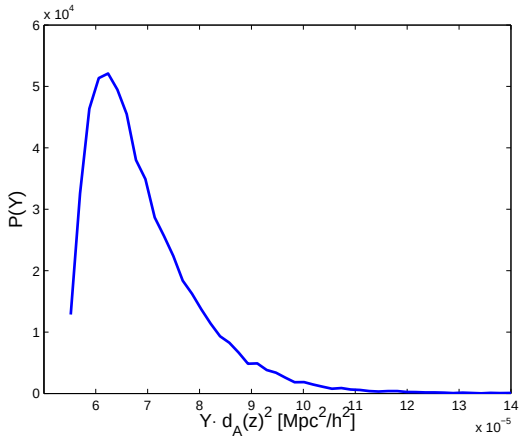

Figure 7. PDF of the integrated Comptonization parameter from the merger-tree model for $M = 10^{15}h^{-1}M_{\odot}$ at $z = 0.01$.

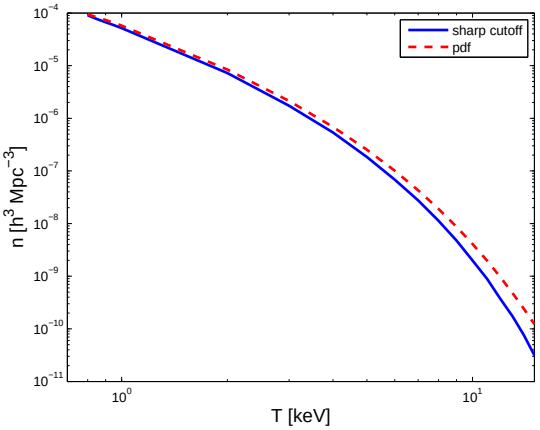

Figure 8. Temperature number counts: the number density of clusters above a certain temperature at $z = 0.1$

formed uncharacteristically early. We note that a log-normal distribution is a poor fit to the outcome of our model.

As in the case of IC gas temperature, scaling relations of the mean values of Y can be computed. The scaling with mass is $Yd_A(z)^2 \propto M^{\delta}$ where $d_A(z)$ is the angular diameter distance and δ varies with redshift, from $\delta = 1.61$ for $z = 0.01$ to $\delta = 1.64$ for $z = 2$. This scaling is close to the standard result $\delta = 5/3$. Similarly, the Comptonization parameter scales with redshift as $Yd_A(z)^2 \propto [E^2(z)\Delta_V(z)]^{\varepsilon}$ with $\varepsilon = 0.26$ for $M = 10^{14}h^{-1}M_{\odot}$ and $\varepsilon = 0.31$ for $M = 10^{16}h^{-1}M_{\odot}$. The evolution with redshift is slower than in the standard description where $\varepsilon = 1/3$.

3.7 Temperature number counts

The PDFs of cluster observables presented above provide a theoretical basis for comparisons with results of cluster surveys. As an example we consider here the predicted temperature number counts, which is one of the statistical cluster functions that can be used to determine cosmological parameters.

The temperature function, that is the cumulative number density of clusters above a certain temperature at a given redshift (interval) is computed from the following expression

$$n(T_i) = \int_{M_{low}}^{M_{high}} B(T_i|M,z)\frac{dn(M,z)}{dM}dM, \qquad (20)$$

where $dn(M,z)/dM$ is the mass function, namely the number of halos per unit comoving volume per unit mass. The selection function $B(T_i|M,z)$ is usually defined as $B = 1$ if $T(M,z) > T_i$ and $B = 0$ otherwise, where $T(M,z)$ is found according to the standard scaling relations (with a sharp cutoff).

However, in accord with our treatment here, there is no one-to-one correspondence between temperature and mass, so we need to incorporate the PDF of the temperature in the calculation of the number counts by using the following selection function

$$B(T_i|M,z) = \int_{T_i}^{\infty} P(T|M,z)dT. \qquad (21)$$

The temperature PDF is described by a log-normal distribution with expectation value and variance taken from best fits to the results of our model. The temperature functions calculated with our more realistic temperature PDF and that with the standard relation (between temperature and mass) are shown in Figure 8. In the standard calculation we chose $T(M,z)$ to equal the expectation value of the respective PDF. The calculations were performed over the mass range $10^{13} - 10^{16}h^{-1}M_{\odot}$ using the Sheth-Tormen mass function.

The two calculations coincide for low temperatures, but for high temperatures our improved treatment yields appreciably higher number counts. The reason for this is that our more exact treatment takes into account the long tails of the distribution functions. Thus, low-mass clusters with mean temperatures below T_0, that do not contribute to $n(T_0)$ when the standard scaling is used, can have a significant overall contribution when the temperature PDF is used. As discussed earlier, this is due to the non-zero probability that the formation redshifts of these clusters, and hence also their temperatures, were higher than the mean values.

As we have mentioned earlier, the log-normal distribution is a mediocre fit to the PDFs of high-mass clusters, and a better understanding of their shapes is required in order to fully assess their impact on temperature number counts. The above calculation demonstrates the importance of taking temperature PDFs into account in the analysis of cluster surveys.

3.8 Model uncertainties

In the previous sections we have shown that our method for the determination of the PDFs of the various cluster physical parameters provides a relatively simpler procedure to implement than hydrodynamical simulations. The procedure involves specifying several free parameters: q - the maximal major merger ratio, κ - the parameter that determines the initial distance between clusters, and the adiabatic index of the gas, Γ. We should also add to this list the parameters of the initial $c(M,z)$ chosen for the smallest halos in the tree (see equation (6)). These parameters were found not to influence the results considerably when chosen reasonably, in accordance with observational results and N-body simulations; see the discussion at the end of Section 3.3.

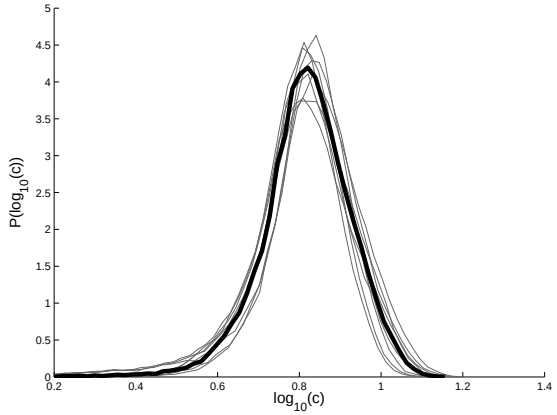

Figure 9. Concentration parameter PDF from the merger-tree model for $M = 10^{15}h^{-1}M_{\odot}$ at $z = 0$ and model parameters in the range $q = 7 - 13$ and $\kappa = 4 - 6$. The thick curve shows the PDF calculated with the fiducial values.

Since we are mainly interested in the global properties of the cluster, such as the emission weighted temperature and the integrated Comptonization parameter, our results have a very weak dependence on a particular choice for the IC gas profile. We have repeated our calculations using the β-profile for the gas:

$$\rho(r) = \rho_{g0}\left[1 + \left(\frac{r}{r_c}\right)^2\right]^{-3\beta/2} \tag{22}$$

with $\beta = 2/3$. The gas core radius is given by $r_c = r_s/\eta$ where r_s is the DM scale radius, and a typical value is $\eta = 2$ (Ricker and Sarazin, 2001). We have integrated the equation of hydrostatic equilibrium to obtain the gas temperature profile, setting the pressure to zero at infinity. With this profile, the temperature PDFs change by just a few percent relative to the polytropic model. We repeated the calculation using also the β-profile with a different boundary condition, namely setting the gas temperature at the virial radius to the temperature of the IGM, typically $10^6 - 10^7$ K. This too had only a minor impact on the results.

In order to estimate the robustness of our model we compute the errors on the PDFs that result from small deviations from the fiducial values of the main model parameters. Figure 9 shows the PDF calculated with parameters in the range $q = 7 - 13$, $\kappa = 4 - 6$.

Other relevant features of the PDF are the expectation value and its variance. These quantities, especially for the temperature and Comptonization parameter, need to be known in the analysis of cluster surveys. We thus need to determine the uncertainty in their values due to variations of model parameters. Varying the parameters in the range $q = 7-13$, $\kappa = 4-6$, $\Gamma = 1.1-1.3$ we obtain $< T >= 9.9^{+0.9}_{-1.4}$ keV for $M = 10^{15}h^{-1}M_{\odot}$ at $z = 0$, while the width of the distribution is $\sqrt{< (T- < T >)^2 >} = 1.4^{+0.2}_{-0.3}$ keV. This likely is a conservative estimate for the range of the temperature uncertainty.

The evolution of the variance of the PDF with mass and redshift and its uncertainty can also be estimated. For instance, if the parameters are varied in the same range $q = 7 - 13$, $\kappa = 4 - 6$, $\Gamma = 1.1 - 1.3$, and for the same mass of $M = 10^{15}h^{-1}M_{\odot}$ but for observation redshift of $z = 0.5$, the following values are obtained: $< T >= 12.0^{+1.0}_{-1.6}$ keV and $\sqrt{< (T- < T >)^2 >} = 1.6 \pm 0.3$ keV. The results for a mass of $M = 10^{14}h^{-1}M_{\odot}$ at redshift $z = 0$ are: $< T >= 2.5^{+0.3}_{-0.4}$ keV and $\sqrt{< (T- < T >)^2 >} = 0.5^{+0.1}_{-0.09}$ keV. The relative uncertainties in all these cases are similar.

Finally, we can estimate the robustness of our results for the evolution of the scaling relations. As an example, we have checked how the scaling of the temperature with mass ($T \propto M^{\zeta}$) and redshift ($T \propto [E^2(z)\Delta_V(z)]^{\lambda}$) changes when the model parameters are varied in the range $q = 7-13$, $\kappa = 4-6$, $\Gamma = 1.1-1.3$. It turns out that ζ and λ change by no more than 1% and 6%, respectively, relative to the values obtained in Section 3.5.

4 DISCUSSION

We have presented an expanded merger-tree treatment for the evolution of galaxy clusters that supplements the statistical description of the dynamical evolution of DM halos with basic physical considerations that enable us to describe also the properties of IC gas. It should be stressed again that our approach is statistical by construction and is not meant to provide a prescription for determining the structure of individual halos, but rather to serve as a tool for studying the properties of a population of clusters. While our treatment is essentially adiabatic, we have adopted an observationally-deduced value of the polytropic index. By doing so we partly compensate for the fact that gas cooling is not explicitly taken into account. Additional justification for the validity of our approach is the fact that we are interested here only in statistical properties of the cluster population, rather than in detailed spatial profiles of the gas density and temperature in individual (such as cooling-core) clusters.

We also assumed that the DM mass profile is not affected by the IC gas. Although this approximation is often made in studies of the statistical properties of a population of clusters (e.g. Bode, Ostriker & Vikhlinin 2009), it is likely to be inaccurate when radiative cooling is important, or when there is energy exchange between the DM and the gas components, for example during mergers. Numerical simulations (Duffy et al. 2010) show that there is a deviation of at most 15% in the concentration parameter of groups and clusters when baryonic physics is included, relative to the DM only case. The impact of IC gas cooling on the DM density profile is often described by adiabatic contraction models (e.g. Gnedin et al. 2004). However, the assumption made in these models that the baryons initially trace the DM distribution is violated during hierarchical build-up of halos. Indeed, Duffy et al. (2010) found that results of the simulations were not well described by adiabatic contraction models beyond $0.1R_{vir}$. A natural extension of our model would be to incorporate IC gas in the halos that constitute the merger tree and to follow the joint evolution of both components.

We calculated the PDFs of the cluster concentration parameter, its IC gas temperature, and integrated Comptonization parameter for different masses and redshifts of observation. Our deduced PDF of the concentration parameter is well fit with a log-normal distribution, in accord with results from N-body simulations. The tempera-

ture PDF for masses below $M \sim 2 \cdot 10^{15} h^{-1} M_{\odot}$ can also be described with a log-normal distribution. Our deduced mass-observable scaling relations are close to the standard relations but contain some corrections - notably the evolution of IC gas temperature with redshift is slower than in the simple model. The results suggest that the gas temperature is not a separable function of mass and redshift. We show a possible application of our results to the analysis of cluster surveys by calculating IC gas temperature number counts, taking into account the effect of cluster formation history.

The probability density functions of the various observables can have important effects on the error estimation in the analysis of cluster X-ray and SZ surveys. As shown by Lima and Hu (2005), large uncertainties in the observable-mass distributions may substantially degrade the constraints on cosmological parameters from cluster surveys. The physically-based estimates of the PDFs of the observables considered here provide a tangible basis to begin addressing this aspect.

Among the other related applications of the approach presented here a particularly timely one is the calculation of the SZ power spectrum, which will be mapped by the *Planck* satellite and several ground-based SZ projects. Comparisons of results from our merger-tree approach and those from simulations and semi-analytical treatments (e.g., see Sadeh, Rephaeli & Silk 2007 and references therein) will yield important insight that will help gauging the relative merits and disadvantages of these very different approaches.

AKNOWLEDGEMENTS

The authors wish to thank the GALFORM team for making the code publicly available. This research was supported by a US-Israel Binational Science Foundation grant 2008452.

REFERENCES

Arnaud, M., Pointecouteau, E., Pratt, G. W. 2005, A&A, 441, 893
Broadhurst, T. J., et al. 2008, ApJ, 695, L9
Bullock, J. S., et al. 2001, MNRAS, 321, 559
Cole, S., Lacey, C. 1996, MNRAS, 281, 716
Cole, S., et al. 2000, MNRAS, 319, 168
Cunha, C. E., Evrard, A. E., 2009, Phys. Rev. D, 81, 083509
Duffy, A. R., et al. 2008, MNRAS, 390, L64
Duffy, A. R., et al. 2010, MNRAS, 405, 2161
Gao, L., et al. 2008, MNRAS, 387, 536
Gnedin, O. Y., et al. 2004, ApJ, 616, 16
Jenkins, A., et al. 2001, MNRAS, 321, 372
Kotov, O., Vikhlinin, A. 2005, ApJ, 633, 781
Lee, J., Komatsu, E. 2010, ApJ, 718, 60
Lima, M., Hu, W., 2005, Phys. Rev. D, 72, 043006
Łokas, E. L., Mamon, G. A., 2001, MNRAS, 321, 155
McCarthy, I. G., et al. 2007, MNRAS, 376, 497
Navarro, J. F., Frenk, C. A., White, S. D. M., 1995, MNRAS, 275, 720
Navarro, J. F., Frenk, C. A., White, S. D. M., 1996, ApJ, 462, 563
Neto, A. F., et al. 2007, MNRAS, 381, 1450
Ostriker, J. P., Bode, P., Babul, A., 2005, ApJ, 634, 964
Parkinson, H., Cole, S., Helly, J. 2008, MNRAS, 383, 557
Press, W. H., Schechter, P. 1974, ApJ, 187, 425
Pratt, G. W., et al. 2009, A&A, 498, 361
Randall, S. W., Sarazin, C. L. 2002, ApJ, 577, 579
Ricker, P. M., Sarazin, C. L. 2001, ApJ, 561, 621
Sadeh, S., Rephaeli, Y. 2008, MNRAS, 388, 1759
Sadeh, S., Rephaeli, Y., Silk, J. 2007, MNRAS, 380, 637
Sarazin, C. L. 2002, in Merging Processes in Clusters of Galaxies, ed. L. Feretti, I. M. Gioia, G. Giovannini (Dordrecht: Kluwer), 1
Sheth, R. K., Tormen, G. 2002, MNRAS, 329, 61
Springel, V., et al. 2005, Nature, 435, 629
Tinker, J., et al. 2008, ApJ, 688, 709
Vikhlinin, A., et al. 2006, ApJ, 640, 691
Vikhlinin, A., et al. 2009a, ApJ, 692, 1033
Vikhlinin, A., et al. 2009b, ApJ, 692, 1060
Voit, G. M., Donahue, M., 1998, ApJ, 500, L111
Wang, J. et al. 2010, preprint (astro-ph/1008.5114)
Wechsler, R. H., et al. 2002, ApJ, 568, 52
Wick, D. R., et al. 2008, ApJ, 680, 17
Zitrin, A. et al. 2009, ApJ, 707, L102

This paper has been typeset from a TEX/ LATEX file prepared by the author.